Assessment of Collagen-Induced Arthritis Using Cyanine 5.5 Conjugated with Hydrophobically Modified Glycol Chitosan Nanoparticles: Correlation with 18F-Fluorodeoxyglucose Positron Emission Tomography Data

Ji Hyeon Cha, MD[1], Sang Hoon Lee, MD[1], Sheen-Woo Lee, MD[1], Kyeongsoon Park, PhD[2],
Dae Hyuk Moon, MD[3], Kwangmeyung Kim, PhD[2], Sandip Biswal, MD, PhD[4]

Departments of [1]Radiology and Research Institute of Radiology and [3]Nuclear Medicine, Asan Medical Center, University of Ulsan College of Medicine, Seoul 138-736, Korea; [2]Korea Institute of Science and Technology, Biomedical Research Center, Seoul 136-791, Korea; [4]Department of Radiology, Division of Musculoskeletal Imaging, Stanford University School of Medicine, Stanford, CA 94305, USA

Objective: To evaluate the potential and correlation between near-infrared fluorescence (NIRF) imaging using cyanine 5.5 conjugated with hydrophobically modified glycol chitosan nanoparticles (HGC-Cy5.5) and 18F-fluorodeoxyglucose-positron emission tomography (18F-FDG-PET) imaging of collagen-induced arthritis (CIA).

Materials and Methods: We used 10 CIA and 3 normal mice. Nine days after the injecting collagen twice, microPET imaging was performed 40 minutes after the intravenous injection of 9.3 MBq 18F-FDG in 200 μL PBS. One day later, NIRF imaging was performed two hours after the intravenous injection of HGC-cy5.5 (5 mg/kg). We assessed the correlation between these two modalities in the knees and ankles of CIA mice.

Results: The mean standardized uptake values of 18F-FDG for knees and ankles were 1.68 ± 0.76 and 0.79 ± 0.71, respectively, for CIA mice; and 0.57 ± 0.17 and 0.54 ± 0.20 respectively for control mice. From the NIRF images, the total photon counts per 30 mm^2 for knees and ankles were 2.32 ± 1.54 x 10^5 and 2.75 ± 1.51 x 10^5, respectively, for CIA mice, and 1.22 ± 0.27 x 10^5 and 0.88 ± 0.24 x 10^5, respectively, for control mice. These two modalities showed a moderate correlation for knees ($r = 0.604$, $p = 0.005$) and ankles ($r = 0.464$, $p = 0.039$). Moreover, both HGC-Cy5.5 ($p = 0.002$) and 18F-FDG-PET ($p = 0.005$) imaging also showed statistically significant differences between CIA and normal mice.

Conclusion: NIRF imaging using HGC-Cy5.5 was moderately correlated with 18F-FDG-PET imaging in the CIA model. As such, HGC-Cy5.5 imaging can be used for the early detection of rheumatoid arthritis.

Index terms: HGC-Cy5.5; 18F-FDG PET; Near-infrared fluorescence imaging; Rheumatoid arthritis

INTRODUCTION

Rheumatoid arthritis (RA) is one of the most frequently diagnosed inflammatory joint diseases. Early diagnosis is the prerequisite of proper therapy in RA, and the diagnosis should be followed by a therapy regimen. Thus, modifying the course of the disease and reducing the degree of severe late sequelae, diagnostic approaches that detect early RA are important (1, 2).

Collagen-induced arthritis (CIA) is an animal model of RA that has been widely used to address the pathogenesis of this disease and to validate therapeutic targets. The main pathological features of CIA include proliferative synovitis, with infiltration of polymorphonuclear and mononuclear

cells, pannus formation, cartilage degradation, erosion of bone, and fibrosis. As in RA, pro-inflammatory cytokines, such as tumor necrosis factor-α and interleukin-1β, are abundantly expressed in the arthritic joints of mice with CIA, and a blockade of these molecules reduce disease severity (3, 4).

Although several imaging techniques have been used to diagnose early RA, they are generally limited to delineating lesions at the anatomical level. Most currently used clinical imaging methods, such as X-ray, computed tomography, magnetic resonance imaging (MRI), and ultrasound rely predominantly on energy/tissue interactions. ^{18}F-fluorodeoxyglucose-positron emission tomography (^{18}F-FDG-PET), a metabolically-based imaging method, has shown significant ^{18}F-FDG uptake in RA joints because of inflammatory processes. Moreover, positive ^{18}F-FDG uptake has been found to correspond to early synovial swelling, and to correlate with ultrasound results (5, 6). MRI has to been known to be the best soft tissue contrast in anatomic imaging, but the field of view is limited in assessing multiple joints, and ^{18}F-FDG-PET can evaluate whole joints as well as quantify the degree of inflammation (7). Hence, we selected ^{18}F-FDG-PET as the gold standard method of this study.

Recently, near-infrared fluorescence (NIRF) imaging, using native cyanine 5.5 (Cy5.5), fluorochrome-labeled antibodies, and indocyanine green or carbocyanine dyes has been used to detect early arthritis in a murine model, indicating that this method may be suitable for the detection of inflammatory joints (8-10).

The natural polyaminosaccharide, chitosan, is a non-toxic, biocompatible, biodegradable, and poorly immunogenic biopolymer (11). Specific antibody targets for arthritis have been developed and contribute to improving diagnosis (10, 12, 13). Exogenous antibodies or proteins, however, can elicit an immune response, which may lead to side-effects or loss of efficacy (14). Thus, a contrast agent for perfusion or permeability could be of benefit in the imaging of patients with RA.

NIR fluorescent polymeric particles labeled with Cy5.5 are suitable for optical imaging because of their relatively long wavelength and their minimal absorbance by hemoglobin, lipids, water, and other tissues in the NIR region (15, 16). In addition, hydrophobically modified glycol chitosan nanoparticles conjugated with Cy5.5 (HGC-Cy5.5) have been found to reach high local concentrations within active angiogenic tissues, such as tumors (17), suggesting that

these HGC nanoparticles may also accumulate in arthritic joints. As a nonspecific contrast agent, HGC-Cy5.5 will accumulate in areas of increased vascularity and vascular leakiness, which are characteristics of arthritic joints. Additionally, fluorescence imaging can quantify the signal intensity of the lesions. Finally, we have evaluated the effectiveness of NIRF imaging using HGC-Cy5.5 to detect early CIA, and compared these results with those of ^{18}F-FDG-PET imaging in a murine model.

MATERIALS AND METHODS

The study was approved by the Institutional Committee on Animal Research.

Animals and Induction of Arthritis

Ten male DBA/1J mice (age 9-10 weeks, weight 20-25 g) were used for the CIA model (20 knees and 20 ankles) and 3 DBA/1J mice were used as normal controls (6 knees and 6 ankles). In the CIA model, mice were injected in the subcutaneous region of the tail with 100 μg bovine type II collagen (5 mg/mL; Chondrex, Redmond, WA, USA) emulsified in an equivalent volume of Freund's complete adjuvant, followed three weeks later by a booster injection of 100 μg bovine type II collagen emulsified in Freund's incomplete adjuvant. RA developed 1 week after the second injection. Nine days after the second injection, ^{18}F-FDG-microPET, and one day after, NIRF imaging were performed.

Preparation of Hydrophobically Modified Glycol Chitosan (HGC) Conjugates Labeled with Cy5.5

Glycol chitosan (Mw = 250 kDa; degree of deacetylation = 82.7%) and 5β-cholanic acid were purchased from Sigma-Aldrich (St. Louis, MO, USA), while the thermo reactive hydroxysuccinimide ester of Cy5.5 was purchased from Amersham Biosciences (Piscataway, NJ, USA). HGC conjugates were modified by chemically conjugating the amine groups of glycol chitosan with the carboxylic group of 5β-cholanic acid (18). HGC particles were labeled with Cy5.5 by chemically coupling 1 wt. % of the hydroxysuccinimide ester of Cy5.5 to glycol chitosan-cholanic acid conjugates dissolved in DMSO at room temperature in the dark for 6 hours. Unreacted Cy5.5 molecules were removed by dialysis for 2 days (molecular weight cutoff = 7 kDa), and the Cy5.5 glycol chitosan conjugate was lyophilized. The Cy5.5 concentration in each glycol chitosan conjugate was similar (0.7 wt. %), as determined by measuring the extinction

coefficient at 675 nm (2.5×10^5 M^{-1} cm^{-1}), according to the manufacturer's instructions.

The morphological shapes of HGC and DTX-HGC nanoparticles were confirmed by transmission electron microscopy (TEM) (CM30 electron microscope, Philips, Eindhoven, the Netherlands), and operated at an acceleration voltage of 80 kV. Each sample (1 mg/mL in distilled water) was placed on a 300-mesh copper grid coated with carbon. Negative staining was performed using a droplet of 2% (w/v) uranyl acetate.

Fluorescence Imaging

The position of all images was acquired at prone and frog leg position for the good exposure of knee and ankle joints. The HGC-Cy5.5 probe (23 wt. %; 5 mL/kg) was injected intravenously (i.v.) into the tail veins of mice, and the biodistribution and joint accumulation of HGC-Cy5.5 were monitored. All mice were shaved around the knee joint for the better evaluation of NIRF imaging. NIRF imaging was performed 2 hours after i.v. injection of the HGC-Cy5.5 probe. Mice were positioned on an animal plate heated to 36°C in the eXplore Optix system (ART Advanced Research Technologies Inc., Montreal, Canada). Laser power and count time settings were optimized at 25 µW and 0.3 s per point. The excitation and emission spots were raster-scanned in 1 mm steps over the selected region of interest to generate emission wavelength scans. A 670 nm pulsed laser diode was used to excite the Cy5.5 molecules, and NIRF emission was monitored at 700 nm. To evaluate HGC accumulation, a dynamic time curve of fluorescence intensity was acquired using a Kodak image station 4000 MM (Kodak, New Haven, CT, USA) every 20 seconds, beginning immediately after HGC-Cy5.5 injection and ending 120 minutes after injection. Accumulation of glycol chitosan nanoparticles was confirmed by measuring NIRF intensity at each joint. Mean fluorescence signal intensities were determined at knee and ankle joints (region of interest [ROI]; 30 mm^2) using an Analysis Workstation software (ART Advanced Research Technologies Inc., Montreal, Canada) (18).

^{18}F-FDG-PET Imaging

^{18}F-fluorodeoxyglucose-positron emission tomography imaging was performed using the MicroPET scanner focus 120 (Siemens Medical Solutions inc., Erlangen, Germany). The covering field of view was 7.6 cm. Mice were injected in the lateral tail vein with 9.3 MBq of ^{18}F-FDG in 200 µL

PBS. After a resting period of 40 minutes to allow uptake of FDG, mice were transferred to the scanning room. The mice were placed in the prone position, and whole body imaging was performed at a suitable single bed position; acquisition time was about 10 minutes. From the ^{18}F-FDG dose and weight of each mouse, we calculated a mean standardized uptake value (mean SUV) as activity (Bq/g)/(injected activity [Bq]/body weight [g]). All data were calculated using a circular ROI with a 3 mm diameter and analyzed using microPET Data Analysis Software (ASIPro VM).

Confocal Laser Scanning Microscopy

Collagen-induced arthritis and normal mice were sacrificed immediately after the NIRF image acquisition. Their knee joints were removed, imbedded in the OCT compound (Miles Scientific), and snap-frozen in liquid nitrogen. Each sample was sectioned at 7 µm thickness with a cryostat and the distribution of HGC-Cy5.5 was evaluated by confocal laser scanning microscopy (LSM510 NLO; Zeiss, Zurich, Germany).

Statistical Analysis

Following calculation of the mean SUV of ^{18}F-FDG-PET and the mean fluorescence signal of NIRF in CIA and normal mice, we assessed the correlation coefficients separately for knees and ankles in CIA mice using Pearson's correlation coefficient. The Mann-Whitney U test was used to assess the differences in mean SUV and mean fluorescence signal between CIA and normal mice.

RESULTS

The chemical structure of HGC-Cy5.5 is shown in Figure 1. A TEM image of HGC-Cy5.5 showed that it consisted of round particles, with an average diameter of 230 nm (Fig. 2). A time intensity curve of the mean photon counts of HGC-Cy5.5 in CIA mice showed a plateau at 20 minutes after injection, which was maintained until 120 minutes after injection (Fig. 3).

The mean SUVs of ^{18}F-FDG for knees and ankles were 1.68 ± 0.76 (average ± SD) and 0.79 ± 0.71, respectively, for CIA mice; and 0.57 ± 0.17 and 0.54 ± 0.20, respectively, for control mice. From NIRF images, the total photon counts per 30 mm^2 for knees and ankles were $2.32 \pm 1.54 \times 10^5$ and $2.75 \pm 1.51 \times 10^5$, respectively, for CIA mice, and $1.22 \pm 0.27 \times 10^5$ and $0.88 \pm 0.24 \times 10^5$, respectively, for control mice. HGC-Cy5.5 uptake was significantly higher in CIA lesions in a murine model than in control joints, with the
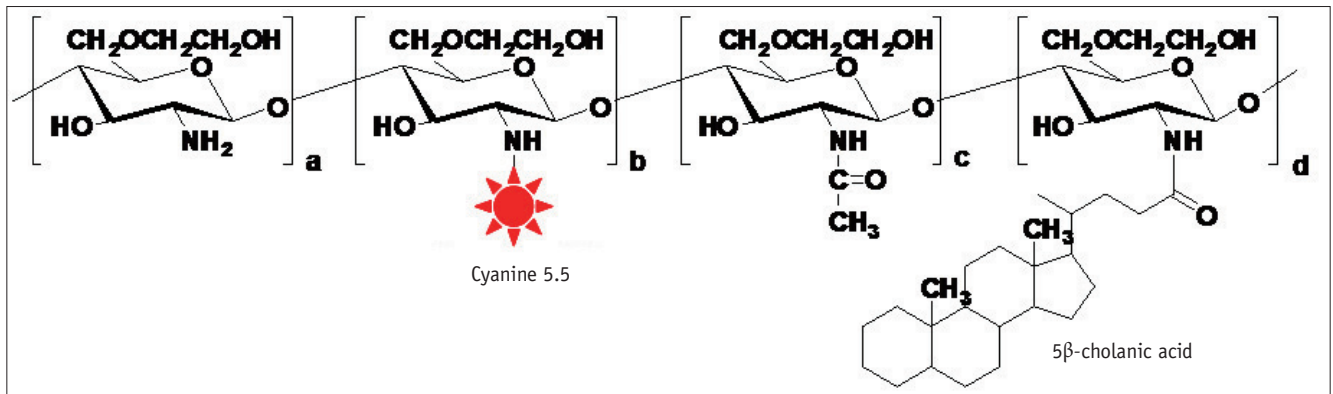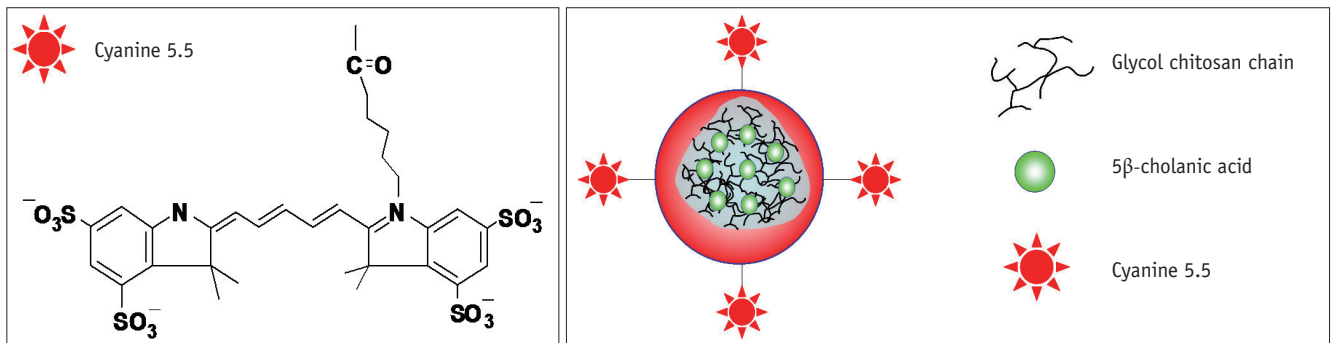
Fig. 1. Chemical structures and in this study.
A. Chemical structure of Cyanine 5.5-labeled hydrophobically modified glycol chitosan (HGC-Cy5.5) conjugates. **B.** Chemical structure of cyanine 5.5. **C.** Schematic diagram of HGC-Cy5.5 nanoparticles
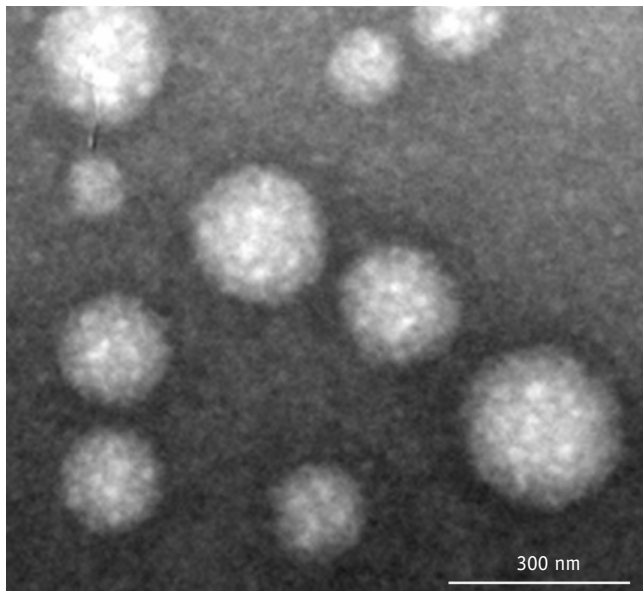

Fig. 2. Transmission electron microscopy images of hydrophobically modified glycol chitosan nanoparticles.

average increase in uptake being 90% in affected knees and 213% in affected ankles. These two imaging modalities showed moderate correlations for knees ($r = 0.604$, $p =$

0.005) and ankles ($r = 0.464$, $p = 0.039$). Both HGC-Cy5.5 ($p = 0.002$) and ^{18}F-FDG-PET imaging ($p = 0.005$) also showed statistically significant differences between CIA and normal mice, but showed large overlap in range (Fig. 4) because all knee and ankle joints were included after twice injection of CIA model even though not every joint developed arthritis in the CIA model. Normal mice showed low FDG and florescence uptake for both knees and ankles (Fig. 5), whereas CIA, in contrast, mice showed significantly higher FDG and photon uptake for both knees and ankles (Fig. 6).

Confocal laser scanning microscopy of arthritic knees showed that HGC-Cy5.5 nanoparticles were distributed in the synovial and subsynovial layers as a bright red color (Fig. 7). No HGC-Cy5.5 nanoparticles were detected in normal knees.

DISCUSSION

We have shown here that HGC-Cy5.5 uptake was significantly higher in CIA lesions in a murine model than in control mice, with the average increase in uptake being 90% in affected knees and 213% in affected ankles. Hansch

et al.(8) reported the increase uptake of the knee joints seen by NIRF was only 64% higher 2 hours after injection of Cy5.5. In contrast to Cy5.5, which binds covalently to
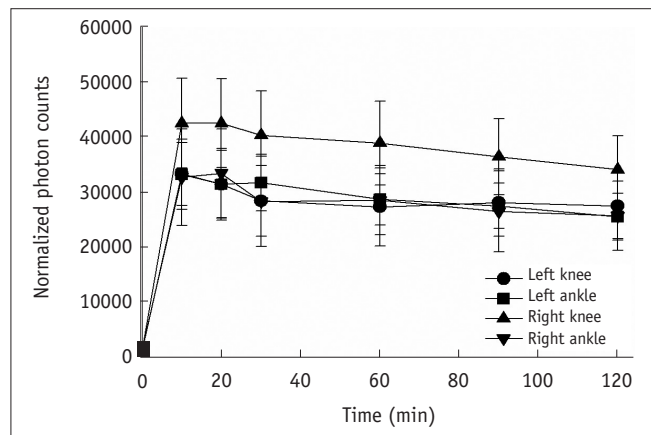

Fig. 3. Time intensity curve for mean photon counts of cyanine 5.5 conjugated with hydrophobically modified glycol chitosan nanoparticles in collagen-induced arthritis mice.

proteins, HGC-Cy5.5 may have a different biodistribution and life cycle *in vivo*. These findings indicate that HGC-Cy5.5 uptake may be more sensitive than NIRF in the detection of murine CIA lesions.

Indocyanine green has been clinically used and approved to assess hepatic function and for fluorescence angiography in ophthalmology (19, 20). This dye, however, is rapidly cleared from the blood by the liver, which limits its ability to reach a target. Compared with indocyanine green, cyanine dyes have been found to show better tissue uptake and slower clearance (21).

We found that HGC nanoparticles accumulated in the synovial and subsynovial layers of arthritic knees. In a tumor model, HGC nanoparticles showed high tumor uptake and low trapping by the liver and spleen (18). The biodistribution of these particles was unexpected, in that smaller micelles were more efficacious than larger ones, whereas larger liposomes (> 200 nm in diameter) showed
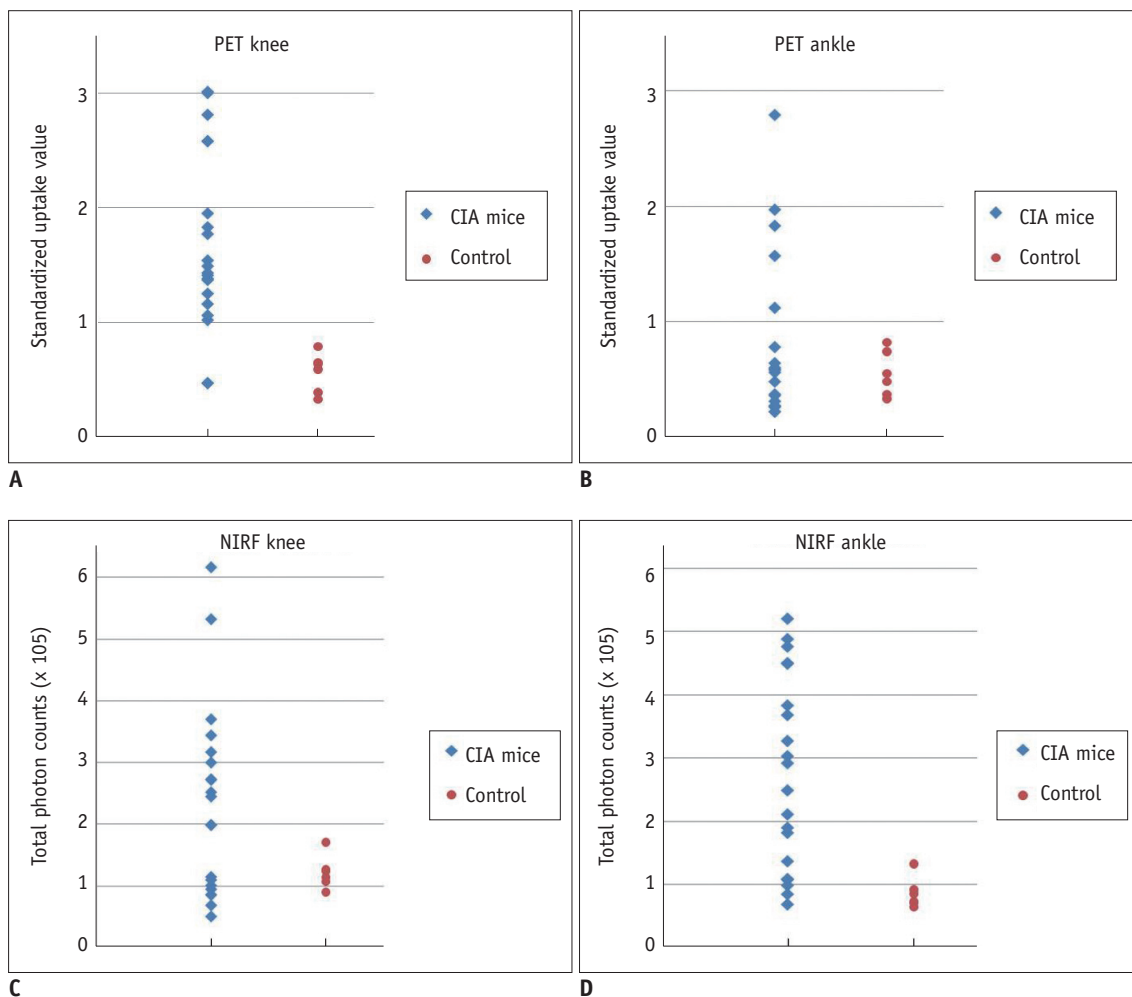

Fig. 4. Diagrams showing results of this study.
Results of ^{18}F-fluorodeoxyglucose-micro positron emission tomography uptake in knee joint **(A)** and ankle joint **(B)**. Near infrared fluorescence uptake in knee joint **(C)** and ankle joint **(D)**.

Fig. 5. Results of ^{18}F-fluorodeoxyglucose-micro positron emission tomography imaging (A) and near-infrared fluorescence imaging (B) using cyanine 5.5 conjugated with hydrophobically modified glycol chitosan nanoparticles at knees (arrows) and ankles (arrowheads) in normal mice.

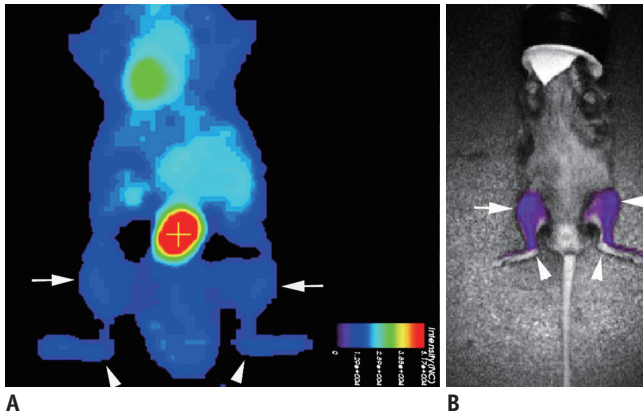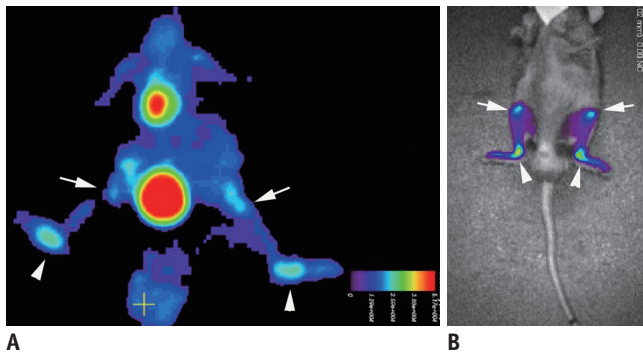**Fig. 6. Results of ^{18}F-fluorodeoxyglucose-micro positron emission tomography imaging (A) and near-infrared fluorescence imaging (B) using cyanine 5.5 conjugated with hydrophobically modified glycol chitosan nanoparticles at knees (arrows) and ankles (arrowheads) in collagen-induced arthritis mice.**

rapid clearance from the RES system because of enhanced RES recognition (18, 22). Coating materials and the hydrophilicity and flexibility of the coating polymer layer may be important in reducing the RES uptake of particles (23). The limited uptake of HGC nanoparticles by the liver and spleen were probably due to the characteristics of chitosan and the deformability of particles in the bloodstream (24).

Non-invasive and functional NIRF imaging systems are emerging as promising diagnostic tools for live animals. These imaging systems are relatively inexpensive, easily accessible, do not generate radiation, and provide quantitative information (16). They have been used to monitor the fate of tumors *in vivo*, thus facilitating the characterization of pathophysiological states (18). Among the various optical imaging systems, NIR light shows the

highest tissue penetration because of minimal uptake by surface tissue of light of the NIR region. Specifically, water, hemoglobin (a principal absorber of visible light), and lipids (primary absorbers of infrared light), show lower uptake of light in the NIR range (15, 16).

The main limitation of fluorescence imaging is that the absolute quantification of target signal is impossible and has depth limitation (25). In this study, ankle joints in arthritic mice showed higher uptake of total photon counts in NIRF imaging than the uptake of knee joints. In contrast, control mice showed lower uptake in ankle joints than knee joints. These might reflect the thick penetration range in the knee joint relative to the ankle joint. Hence, the quantification of NIRF imaging might be limited to the comparison in the same joint or similar penetration depth. Fluorescence molecular tomography could be provided at a deeper depth limitation up to 20 cm (25), such that fluorescence molecular tomography is more reliable for imaging and quantification of living animals or superficial targets of human. RA in humans predominantly affects the small joints of the hand and wrist. Our findings indicate that NIRF imaging of these small joints could become feasible in the near future (10, 12).

[18]F-fluorodeoxyglucose-positron emission tomography imaging shows the metabolic activity of RA. At present, ^{18}F-FDG-PET is not used diagnostically because of high cost and limited accessibility (7). However, ^{18}F-FDG-PET offers unique information on glucose metabolism and is able to detect early inflammation (6, 26), indicating that ^{18}F-FDG-PET may be a promising tool for monitoring RA progress and therapeutic response (7, 27).

We found that ^{18}F-FDG-PET and NIRF using HGC-Cy5.5 yielded data that correlated positively in our CIA murine model. However, neither ^{18}F-FDG nor the HGC-cy5.5 probe is specific for detecting synovial lesions in RA. Activated macrophages are thought to be intimately involved in the pathogenesis of RA by directly destroying articular tissue, secreting matrix metalloproteinases, and attracting or activating other immune cells via the release of cytokines. The quantification of activated macrophages in joint tissues may therefore be of diagnostic value because activated macrophage content correlates well with articular destruction and poor disease prognosis in humans (10, 28).

We found that ^{18}F-FDG uptake was higher in the knees than in the ankles of CIA mice, whereas NIRF imaging showed higher uptake in ankles than in knees. As we mentioned above, comparison of the quantification of
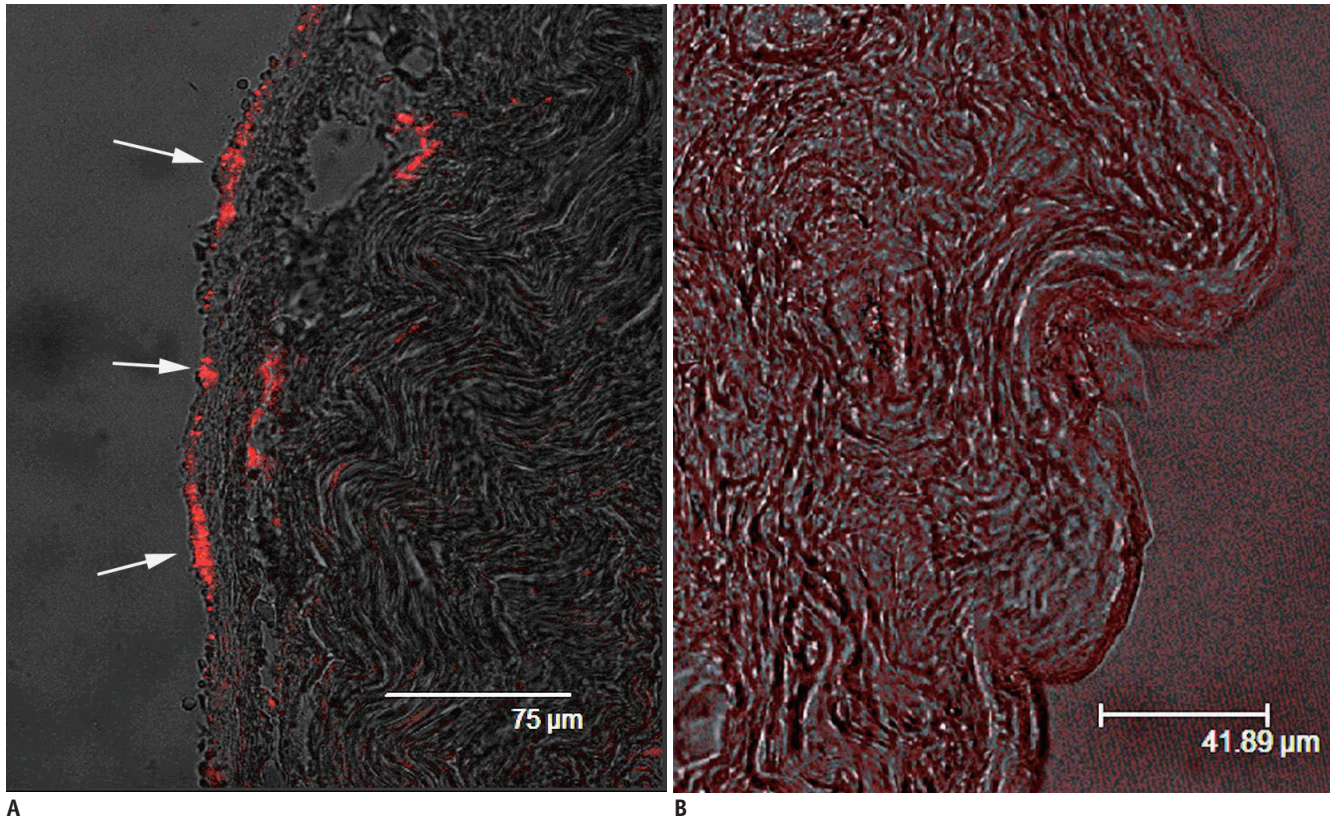
Fig. 7. Confocal laser scanning microscopy of arthritic knee (A) and control knee (B), showing that cyanine 5.5-conjugated, hydrophobically modified, glycol chitosan nanoparticles emit bright red light (arrows) at synovial and subsynovial layers of arthritic knees (x 400 magnification).

NIRF imaging in different joints is limited. Hence, the quantification of different joints is better in ^{18}F-FDG PET imaging. Glucose uptake was increased in early inflammatory arthritis, but glucose metabolism was not correlated with regional blood flow (29). Thus, different imaging data may be related to different uptake values in various joints.

In conclusion, NIRF images using the HGC-Cy5.5 probe showed increased uptake at the joints of CIA mice, and correlated with ^{18}F-FDG-PET imaging. These findings indicate that NIRF images using a high wavelength optical probe may be clinically useful in the detection of RA.

REFERENCES

1. Sommer OJ, Kladosek A, Weiler V, Czembirek H, Boeck M, Stiskal M. Rheumatoid arthritis: a practical guide to state-of-the-art imaging, image interpretation, and clinical implications. *Radiographics* 2005;25:381-398
2. Wunder A, Straub RH, Gay S, Funk J, Müller-Ladner U. Molecular imaging: novel tools in visualizing rheumatoid arthritis. *Rheumatology (Oxford)* 2005;44:1341-1349
3. Holmdahl R, Andersson ME, Goldschmidt TJ, Jansson L, Karlsson M, Malmström V, et al. Collagen induced arthritis as an experimental model for rheumatoid arthritis. Immunogenetics, pathogenesis and autoimmunity. *APMIS* 1989;97:575-584
4. Williams RO. Collagen-induced arthritis as a model for rheumatoid arthritis. *Methods Mol Med* 2004;98:207-216
5. Elzinga EH, van der Laken CJ, Comans EF, Lammertsma AA, Dijkmans BA, Voskuyl AE. 2-Deoxy-2-[F-18]fluoro-D-glucose joint uptake on positron emission tomography images: rheumatoid arthritis versus osteoarthritis. *Mol Imaging Biol* 2007;9:357-360
6. Beckers C, Ribbens C, André B, Marcelis S, Kaye O, Mathy L, et al. Assessment of disease activity in rheumatoid arthritis with (18)F-FDG PET. *J Nucl Med* 2004;45:956-964
7. Brenner W. 18F-FDG PET in rheumatoid arthritis: there still is a long way to go. *J Nucl Med* 2004;45:927-929
8. Hansch A, Frey O, Hilger I, Sauner D, Haas M, Schmidt D, et al. Diagnosis of arthritis using near-infrared fluorochrome Cy5.5. *Invest Radiol* 2004;39:626-632
9. Fischer T, Gemeinhardt I, Wagner S, Stieglitz DV, Schnorr J, Hermann KG, et al. Assessment of unspecific near-infrared dyes in laser-induced fluorescence imaging of experimental arthritis. *Acad Radiol* 2006;13:4-13
10. Chen WT, Mahmood U, Weissleder R, Tung CH. Arthritis imaging using a near-infrared fluorescence folate-targeted

probe. *Arthritis Res Ther* 2005;7:R310-R317

11. Kaş HS. Chitosan: properties, preparations and application to microparticulate systems. *J Microencapsul* 1997;14:689-711

12. Hansch A, Frey O, Sauner D, Hilger I, Haas M, Malich A, et al. In vivo imaging of experimental arthritis with near-infrared fluorescence. *Arthritis Rheum* 2004;50:961-967

13. Sugimoto K, Nishimoto N, Kishimoto T, Yoshizaki K, Nishimura T. Imaging of lesions in a murine rheumatoid arthritis model with a humanized anti-interleukin-6 receptor antibody. *Ann Nucl Med* 2005;19:261-266

14. Frost H. Antibody-mediated side effects of recombinant proteins. *Toxicology* 2005;209:155-160

15. Licha K, Hessenius C, Becker A, Henklein P, Bauer M, Wisniewski S, et al. Synthesis, characterization, and biological properties of cyanine-labeled somatostatin analogues as receptor-targeted fluorescent probes. *Bioconjug Chem* 2001;12:44-50

16. Weissleder R. A clearer vision for in vivo imaging. *Nat Biotechnol* 2001;19:316-317

17. Kim JH, Kim YS, Park K, Kang E, Lee S, Nam HY, et al. Self-assembled glycol chitosan nanoparticles for the sustained and prolonged delivery of antiangiogenic small peptide drugs in cancer therapy. *Biomaterials* 2008;29:1920-1930

18. Park K, Kim JH, Nam YS, Lee S, Nam HY, Kim K, et al. Effect of polymer molecular weight on the tumor targeting characteristics of self-assembled glycol chitosan nanoparticles. *J Control Release* 2007;122:305-314

19. Caesar J, Shaldon S, Chiandussi L, Guevara L, Sherlock S. The use of indocyanine green in the measurement of hepatic blood flow and as a test of hepatic function. *Clin Sci* 1961;21:43-57

20. Brancato R, Trabucchi G. Fluorescein and indocyanine green angiography in vascular chorioretinal diseases. *Semin Ophthalmol* 1998;13:189-198

21. Licha K, Riefke B, Ntziachristos V, Becker A, Chance B, Semmler W. Hydrophilic cyanine dyes as contrast agents for near-infrared tumor imaging: synthesis, photophysical properties and spectroscopic in vivo characterization. *Photochem Photobiol* 2000;72:392-398

22. Storm G, Roerdink FH, Steerenberg PA, de Jong WH, Crommelin DJ. Influence of lipid composition on the antitumor activity exerted by doxorubicin-containing liposomes in a rat solid tumor model. *Cancer Res* 1987;47:3366-3372

23. Takeuchi H, Kojima H, Toyoda T, Yamamoto H, Hino T, Kawashima Y. Prolonged circulation time of doxorubicin-loaded liposomes coated with a modified polyvinyl alcohol after intravenous injection in rats. *Eur J Pharm Biopharm* 1999;48:123-129

24. Hwang HY, Kim IS, Kwon IC, Kim YH. Tumor targetability and antitumor effect of docetaxel-loaded hydrophobically modified glycol chitosan nanoparticles. *J Control Release* 2008;128:23-31

25. Weissleder R, Ntziachristos V. Shedding light onto live molecular targets. *Nat Med* 2003;9:123-128

26. Goerres GW, Forster A, Uebelhart D, Seifert B, Treyer V, Michel B, et al. F-18 FDG whole-body PET for the assessment of disease activity in patients with rheumatoid arthritis. *Clin Nucl Med* 2006;31:386-390

27. Palmer WE, Rosenthal DI, Schoenberg OI, Fischman AJ, Simon LS, Rubin RH, et al. Quantification of inflammation in the wrist with gadolinium-enhanced MR imaging and PET with 2-[F-18]-fluoro-2-deoxy-D-glucose. *Radiology* 1995;196:647-655

28. Bresnihan B. Pathogenesis of joint damage in rheumatoid arthritis. *J Rheumatol* 1999;26:717-719

29. Andersson SE, Johansson A, Lexmüller K, Ekström GM. Physiological characterization of mBSA antigen induced arthritis in the rat. II. Joint blood flow, glucose metabolism, and cell proliferation. *J Rheumatol* 1998;25:1778-1784